

1 **Source parameters and seismic moment-magnitude scaling for Northwestern**
2 **Turkey.**

3 Parolai S. ⁽¹⁾, D. Bindi⁽²⁾, E. Durukal⁽³⁾, H. Grosser⁽¹⁾, and C. Milkereit ⁽¹⁾.

4 (1) GeoForschungsZentrum Potsdam, Telegrafenberg, 14473, Potsdam Germany

5 (2) Istituto Nazionale di Geofisica e Vulcanologia, via Bassini 15, 20133 Milano,
6 Italy

7 (3) Bogazici University, Kandilli Observatory and Earthquake Research Institute,
8 Department of Earthquake Engineering, 34684, Cengelkoy, Istanbul, Turkey

9

10 **Abstract**

11 The source parameters of 523 aftershocks ($0.5 < M_L < 5.9$) of the 1999 Kocaeli earthquake
12 are determined by performing a two-step spectral fitting procedure. The source spectrum,
13 corrected for both site and propagation effects, is described in terms of a standard ω -
14 square model multiplied by an exponential term of frequency. The latter term is
15 introduced to estimate the high frequency ($f > 12\text{Hz}$) fall-off of the acceleration source
16 spectra, by computing the κ parameter. The obtained seismic moments range between
17 1.05×10^{14} and 2.41×10^{17} Nm, while the Brune-stress drops are between 0.002 and 40
18 MPa. κ varies between 0.00 and 0.08 s indicating a decay of the acceleration level at high
19 frequency greater than that assumed by the ω^{-2} model. Both the stress drop and the κ
20 parameter show the tendency of increasing with aftershock magnitude. No evidence of
21 self similarity break down is observed between the source radius and M_0 . Finally, both the
22 seismic moment and the moment magnitude are compared to the local magnitude to
23 derive new moment-magnitude relationships for the area, to be considered for seismic
24 hazard assessment.

25

26

27 **Introduction**

28 On August 17, 1999, a magnitude $M_w=7.4$ earthquake struck the Kocaeli
29 province of Turkey and three months later, on November 12, 1999, the $M_w=7.2$ Düzce
30 earthquake occurred to the immediate east of the fault rupture of the Kocaeli earthquake.
31 Since then, many studies (among many others *Tibi et al.*, 2001, *Eken et al.*, 2004,
32 *Durukal and Catalyürekli*, 2004, *Bindi et al.*, 2006a, *Bindi et al.*, 2006b) have focused on
33 this area. Recent studies (e.g. *Atakan et al.*, 2002; *Erdik et al.*, 2004; *Parsons*, 2004)
34 showed that the segments of the North Anatolia Fault in the Sea of Marmara to the
35 immediate south of Istanbul have a very significant probability (40-65%) of producing a
36 $M>7$ earthquake within the next 30 years that will likely create very high hazard levels in
37 the city of Istanbul. With the recognition of the substantial earthquake hazard and risk
38 levels of Istanbul, many international projects have been initiated with the ultimate aim of
39 mitigating urban earthquake risk. Within the framework of one of these, “Megacity
40 Istanbul”, one objective was to determine the actually lacking source parameter scaling
41 relationships for the area that can then be used both for the simulation of regional strong
42 ground motion (e.g. *Boore*, 2003), and for seismic hazard predictions, using, for example
43 a standard probabilistic approach (Cambiarla con Cornell? *Franceschina et al.*, 2006). In
44 fact, source parameters play a key role in the estimation of attenuation relationships, in
45 the definition of source parameterization for ground motion simulation etc. (necessary?)

46 In this study, source parameters of 523 earthquakes recorded by two seismic
47 networks (German Task Force – GTF and SApancaBOlu -SABO) and a strong motion
48 network (Kandilli Observatory and Earthquake Research Institute -KOERI) are derived.
49 The source spectrum was obtained by means of the generalized inversion technique
50 (*Castro et al.*, 1990; *Bindi et al.*, 2006a) and then fitted in a first step using a Brune-
51 source model (*Brune*, 1970). The fit was also performed in a second step by introducing a
52 high frequency diminution term (*Halldorsson and Papageorgiou*, 2005). The seismic

53 moment was used to derive new empirical relationships with the local magnitude M_L
54 (calibrated for the area by *Baumbach et al.* (2003) and updated recently by *Bindi et al.*,
55 (2006c)). New empirical relationships between seismic moment and source radius, as
56 well as between rms stress drop ($\Delta\sigma_{rms}$) (*Andrews*, 1986) and Brune stress drop ($\Delta\sigma_B$), are
57 also shown. These relationships can be used to guide ground-motion predictions in the
58 area.

59

60 **Data**

61 Amongst the aftershocks recorded by the 53 stations of the GTF, SABO and
62 KOERI networks, the recordings of 523 earthquakes with M_L ranging between 0.5 and
63 5.9 were considered. GTF and SABO networks consist of 1-Hz geophones (Mark L4-
64 3D), a 24-bit digitizer with a sampling rate of 100 sps and Global Positioning System
65 (GPS) timing. The KOERI strong-motion network consist of GeoSys GSR-16 and
66 Kinematics SSA-2 strong motion stations working with sampling rates of 200 sps.

67 The selection of the events was carried out aiming at obtaining satisfactory ray-
68 path coverage (as requested from the generalised inversion technique) of the area from
69 well-located events (Figure 1). The hypocenter locations of the selected earthquakes,
70 calculated using a standard procedure (*Bindi et al.*, 2006c), lead to root mean squares
71 (RMS) values of the travel time residuals smaller than 0.5 s, with an average value of
72 0.13 s. The horizontal and vertical statistical errors are smaller than 1.8 and 2 km,
73 respectively.

74 For all recordings, the Fast Fourier Transform (FFT) of a 5s window of signal,
75 starting 1 second before the S-wave arrival was calculated. If the difference between S-
76 and P-wave arrival time was smaller than 1 second (check how many cases!) the window
77 was shifted in order to avoid the main P-wave arrival energy. Trends from the chosen
78 signal windows were removed, and a 5% cosine taper was applied at both ends before the

79 FFT calculation. Spectra were corrected for the instrumental response of the sensors and
80 smoothed using a *Konno and Ohmachi* (1998) window with $b=20$. Generally b is varied
81 between 10 and 60 with the smaller values determining larger smoothing of the spectra.
82 As a final step of data preparation, the vector sum of the two horizontal and vertical
83 spectra was obtained. The reader is referred to *Baumbach et al.* (2003), *Parolai et al.*
84 (2004), *Bindi et al.* (2006a) and *Bindi et al.* (2006b) for more detailed information about
85 the data set.

86

87 **Method**

88 Source spectra were obtained by the generalized spectra inversion [e.g. *Castro et*
89 *al.*, 1990], that allows the separation of the site, path and source contributions from the
90 observed spectra. This is achieved after having taken the logarithm of the spectra of the
91 recordings – of several earthquakes registered by different stations- and solving the
92 resulting linear system in a least-squares sense. A non-parametric approach was here
93 adopted for the inversion. The distance range covered by the data set (10 to 190 km) was
94 discretized into 60 bins with widths of 3 km. The inversion was performed separately for
95 each of the 70 selected frequency, equi-spaced in logarithmic scale between 0.4 and 25
96 Hz, using the least square algorithm (LSQR) of Paige and Saunders (1982). A detailed
97 description of the inversion can be found in *Parolai et al.* (2004) and *Bindi et al.* (2006a).

98 In order to derive source parameters like seismic moment, corner frequency and
99 $\Delta\sigma_B$ a two-step procedure was followed.

100 In a first step, displacement source spectra were fitted to a ω -square source model with
101 only one corner frequency (*Brune*, 1970), assuming an S-wave velocity of 3.5 km/s, a
102 density of 2800 kg m^{-3} and an average radiation pattern of 0.6. A grid search procedure
103 was applied, where $\Delta\sigma_B$ was varied between 1kPa and 100 MPa, and the seismic moment
104 M_0 over intervals depending on the magnitude. The M_0 intervals ranged between 10^9 Nm

105 and 10^{12} Nm for the smallest analysed events and between 10^{16} Nm and 10^{18} Nm for the
 106 largest ones. In particular, 20 steps per decade (equally spaced in logarithmic scale) were
 107 allowed for both parameters. The cost function to minimize was

$$108 \quad rms = \sqrt{\frac{\sum_1^{N_f} (\log O(f) - \log C(f))^2}{N_f}} \quad (1)$$

109 where $O(f)$ is the observed spectrum, $C(f)$ is the calculated spectrum, and N_f is the number
 110 of considered frequencies. The frequency range considered was 0.5-25 Hz. Although the
 111 spectral fit was generally very good (Figure 2, top panel), it was found that the high-
 112 frequency part of the source spectrum was not completely described by the adopted
 113 function, consistent with the generally observed rapid decay (greater than that assumed
 114 by ω^{-2} model) of the acceleration level at high frequency (*Hanks, 1979; Halldorsson and*
 115 *Papageorgiou, 2005*). Therefore, in a second step, acceleration source spectra were fitted
 116 by considering not only a ω -square model but also a high frequency diminution function
 117 (*Halldorsson and Papageorgiou, 2005*)

$$118 \quad D(f, \kappa) = \exp(-\pi \kappa f) \quad (2)$$

119 Where f is the frequency, and, in this study, κ is a parameter determining the high
 120 frequency source spectral decay. It accounts for the source contribution (*Purvance and*
 121 *Anderson, 2003*) to the parameter κ , defined in *Anderson and Hough (1984)* that is
 122 generally adopted in stochastic simulations of strong ground motion. The second step
 123 constrains M_0 to the value calculated in step 1, and allows for a grid search for $\Delta\sigma_B$ and
 124 κ . After a visual inspection of all the fit results (or spectra?) of step 1, the function $D(f, \kappa)$
 125 was applied from 12 Hz, which for this data set is where the high frequency decay
 126 generally begins. In the grid search procedure, $\Delta\sigma_B$ was varied between 1 kPa and 40
 127 MPa in steps of 0.01 MPa, while κ was varied between 0.0 s and 0.1 s in steps of 0.002 s.
 128 The cost function was defined as in step 1. The excellent final fits (0.09 and 0.06)

129 obtained for two sample events with M_L 5.5 and 2.1, respectively, are shown in Figure 2,
130 bottom panel.

131

132 **Results**

133 Before discussing into details the relationships between the parameters obtained
134 from the two-step procedure, an inspection to the *rms* values (Figure 3) provides
135 information on the accuracy of their estimation. The values are quite small, with the
136 great majority being less than 0.2. Less accurate fits ($rms > 0.2$) were obtained for higher
137 magnitude events ($M_L > 3.5-4$), indicating problems in the adopted procedure when the
138 corner frequency (f_c) of the event is closer to the lower bound of the analysed frequency
139 band. A strong reduction of *rms* reached after the second step when the fit was performed
140 considering also κ is evident, confirming that the use of the high-frequency diminution
141 function $D(f, \kappa)$ is appropriate. The average *rms* after the second step of the procedure
142 decreases from 0.127 ± 0.048 to 0.079 ± 0.029 .

143 The κ values range between 0.00 and 0.08 s, showing a clear tendency to increase with
144 M_L . Note that the site and path effects were removed from the fitted source spectra by the
145 generalized inversion technique. The positive correlation between κ and M_L (the best
146 fitting, in a least-squares sense line has a slope equal to 0.0071 ± 0.0005) agrees with the
147 results obtained by Bindi et al (2006b), who inverted κ values estimated directly from the
148 observed acceleration spectra, so as to isolate the site, source and path contributions,
149 without introducing any source model. They also found that the source contribution to κ
150 correlates with M_L , with the least-squares fit of the results giving a slope equal to 0.0051.
151 The high scatter in the distribution of κ against M_L shown in Figure3, implies a
152 correlation coefficient $R=0.5086$, with a null hypothesis of no-correlation between the
153 two parameters that can be rejected at a 0.98 level of confidence by performing a t-
154 Student test.

155 Figure 4 shows graphically the scaling between f_c and M_L and that between M_0 and
156 the Brune source radius. A clear scaling of the corner frequency with M_L is observed
157 within the full magnitude range considered ($0.5 < M_L < 5.9$). This is reflected in the scaling
158 of the source radius versus the M_0 , where the source radius varies from nearly 100 m to
159 2.5 km. Consistent with previous studies (e.g. *Abercombie, 1995; Franceschina et al.,*
160 *2006*) no evidence of self similarity break down is observed within the range of M_0
161 investigated ($1.05 \times 10^{14} < M_0 < 2.41 \times 10^{17}$ Nm). However, a tendency of $\Delta\sigma_B$ (varying
162 between 2 kPa and 40 MPa, but with the great majority of values between 10 kPa and 10
163 MPa) to increase with M_0 is shown in Figure 4. The large scattering shown by the $\Delta\sigma_B$
164 values might be related to the hypocentral location and the focal mechanism.

165 The corner frequency and $\Delta\sigma_{rms}$ were calculated following Andrews (1986), in
166 order to have an independent estimate of the stress drop. In this way, $\Delta\sigma_{rms}$ is calculated
167 directly from the acceleration spectrum without making any assumption about the source
168 function. For a case where the source spectrum is identical to a Brune model, $\Delta\sigma_{rms}$
169 should equal $\Delta\sigma_B$.

170 Figure 5 shows that $\Delta\sigma_B$ appears to be strongly correlated with $\Delta\sigma_{rms}$, where the
171 average of the \log_{10} of the spectral ratio between $\Delta\sigma_{rms}$ and $\Delta\sigma_B$ equals -0.19 ± 0.37 . Since
172 the same ratio calculated using the $\Delta\sigma_B$ from step 1 (also showing a strong correlation
173 with $\Delta\sigma_{rms}$) provided a value of 0.034 ± 0.37 , it appears that, as expected, the introduction
174 of the κ factor leads to a shift toward higher values of $\Delta\sigma_B$.

175 Finally, in Figure 6, M_0 (top) and M_w (bottom), obtained using the equation of
176 *Kanamori (1977)*, are shown versus M_L . A linear orthogonal regression between $\log_{10} M_0$
177 and M_L (black line in Figure 6, top) led to the equation

$$178 \quad \log_{10} M_0 = (1.17 \pm 0.01) M_L + (10.12 \pm 0.02) \quad (3)$$

179 While this relationship is in good agreement with that of *Grosser et al., (1998)* (gray
180 line) calculated from the aftershocks of the Erzican earthquake, it differs to that of

181 *Durukal and Catalyürekli, (2004)* (dashed line). We believe that this disagreement may
182 be due to the use of a M_L scale with coefficients not calibrated for the area in the latter
183 study.

184 Results of the regression between M_w and M_L are shown in Figure 6, bottom. In
185 this case, a non-linear least-squares regression was carried out considering a quadratic
186 term. Since the regression is not orthogonal, it was carried out in two directions,
187 considering in one case M_L , and in the other M_w , as independent variables. Therefore,
188 two relationships obtained are:

$$189 M_w \leftarrow (0.95 \pm 0.03) + (0.58 \pm 0.02)M_L + (0.03 \pm 0.004)M_L^2 \quad (4)$$

$$190 M_L \leftarrow (-9.001 \pm 1.59) + \sqrt{((54.25 \pm 25.94) + (30.19 \pm 4.11)M_w)} \quad (5)$$

191
192 Since the data set shows a strong correlation between M_w and M_L with a very limited
193 scattering of data points, indicating that path and site-effect corrections were efficiently
194 carried out, both relations, when plotted, lead to very similar graphs. That is why in
195 Figure 6, bottom, only equation (4) is shown. The new relationship shows generally a
196 good agreement with the chi-square regression derived by *Stromeyer et al. (2004)* (gray
197 line) for continental Europe. Small discrepancies may be due to the different tectonic
198 regimes of the areas in which the data sets have been collected.

199

200 **Conclusions**

201 New source spectral models for Northwestern Turkey have been calibrated using a large
202 data set of aftershocks (523) following the Kocaeli earthquake. The main results are
203 summarized as follows:

- 204 - Introducing a high frequency diminution function improved the spectral fit with
205 respect to that obtained considering only a Brune source model.

- 206 - The obtained values of κ appear to vary as a function of M_L . The null hypothesis
207 of no-correlation between the two parameters can be rejected at a 0.98 level of
208 confidence by performing a t-Student test.
- 209 - $\Delta\sigma_B$ appears to increase with M_0 in the analyzed seismic moment range
210 ($1.05 \times 10^{14} < M_0 < 2.41 \times 10^{17}$ Nm).
- 211 - $\Delta\sigma_B$ and $\Delta\sigma_{rms}$ appear to be strongly correlated, indicating that the source spectra
212 can be correctly describe by a Brune source model, and that the estimate of f_c are
213 reliable.
- 214 - New relationships between M_L , calibrated for the first time in the area by
215 *Baumbach et al.*, (2003) and updated by *Bindi et al.* (2006c), and M_w , were
216 derived.

217 The large scattering shown by the $\Delta\sigma_B$ values might be related to the hypocentral location
218 and the focal mechanism. This point will be subject of future investigations.

219 The new relationships provide important information about source parameters such as
220 $\Delta\sigma_B$ and κ , and thus can assist efforts to simulate strong ground motion in northwestern
221 Turkey.

222

223 **Acknowledgments**

224 This work was partially funded by the project "Megacity: Istanbul". Part of this work was
225 conducted during the visits of Dino Bindi at the GFZ-Potsdam that were partially funded
226 by the GeoForschungsZentrum Potsdam. K. Fleming kindly improved our English. We
227 thank M. Bohnhoff and E. Gorgun, for having provided part of the arrival time pickings
228 and the earthquake locations. Figures were generated using the Generic Mapping Tools
229 (Wessel and Smith, 1991).

230

231

232 **References**

233 Abercombie, R.E., (1995). Earthquake source scaling relationships from -1 to 5 M_L
234 using seismograms recorded at 2.5 km depth, *J. Geophys. Res.*, 100, 24015-24036.

235

236 Anderson, J. G., and S. E. Hough (1984). A model for the shape of the Fourier amplitude
237 spectrum of acceleration at high frequencies, *Bull. Seism. Soc. Am.*, 74, 1969-1993.

238

239 Andrews, D. J. (1986). Objective determination of source parameters and similarity of
240 earthquakes of different size, In: Das, S., Boatwrigth, J., Scholz, C.H. (Eds.), *Earthquake*
241 *source mechanics*, Am. Geophys. Union, Geophys. Monogr., 37, vol. 6, 259-267.

242

243 Atakan, K., A. Ojeda, M. Meghraoui, A. A. Barka, M. Erdik, and A. Bodare, (2002).
244 Seismic Hazard in Istanbul following the 17 August Izmit and 12 November 1999 Düzce
245 earthquakes, *Bull. Seism. Soc. Am.*, 92, 1, 466-482.

246

247 Baumbach, M., D. Bindi, H. Grosser, C. Milkereit, S. Parolai, R. Wang, S. Karakisa, S.
248 Zünbül, and J. Zschau (2003). Calibration of an M_L scale in Northwestern Turkey from
249 1999 Izmit aftershocks, *Bull. Seism. Soc. Am.*, 93, 5, 2289-2295.

250

251 Bindi D., S. Parolai, H. Grosser, C. Milkereit, and S. Karakisa, (2006a). Crustal
252 attenuation characteristics in northwestern Turkey in the range from 1 to 10 Hz, *Bull.*
253 *Seism. Soc. Am.*, 96, 200-214.

254

255 Bindi D., S. Parolai, H. Grosser, C. Milkereit, and S. Zünbül, (2006b). Cumulative
256 attenuation along source-to-receiver paths in northwestern Turkey, *Bull. Seism. Soc. Am.*,
257 96, 188-199.

258

259 Bindi D., S. Parolai, E. Görgün, H. Grosser, C. Milkereit, M. Bohnhoff, E. Durukal,
260 (2006c). M_L scale in Northwestern Turkey from 1999 Izmit aftershocks: updates,
261 submitted to *Bull. Seism. Soc. Am.*

262

263 Boore, D., (2003). Simulation of ground motion using stochastic method, *Pure Appl.,*
264 *Geophys.*, 160, 635-676.

265

266 Brune, J. N. (1970). Tectonic stress and the spectra of seismic shear waves from
267 earthquakes, *J. Geophys. Res.*, 75, 4997-5009.

268

269 Castro R.R., J.G. Anderson, and S.K Singh (1990). Site response attenuation and source
270 spectra of S waves along the Guerrero, Mexico, subduction zone, *Bull. Seism. Soc. Am.*,
271 80, 1481-1503.

272

273 Durukal E., and Y. Catalyürekly (2004). Spectral analysis of source parameters of the
274 1999 Kocaeli and Düzce earthquake aftershock sequences, *13th WCEE*, Vancouver, B.C.,
275 Canada, August 1-6, 2004, Paper n. 421.

276

277 Eken, T., K. Mayeda, A. Hofstetter, R. Gök, G. Örgülü, and N. Turkelli (2004). An
278 application of the coda methodology for moment-rate spectra using broadband stations in
279 Turkey, *Geophys. Res. Lett.*, 31, L11609, doi:10.1029/2004GL019627.

280

281 Erdik, M., M. Demircioglu, K. Sesetyan, E. Duruka, B. Siyahi (2004). Earthquake hazard
282 in Marmara region, Turkey, *Soil. Dynam. Earthquake Eng.*, 24, 605-631.

283

284 Franceschina G., S. Kravanja and G. Bressan, (2006). Source parameters and scaling
285 relationships in the Friuli-Venezia Giulia (Northwestern Italy) region, *Phys. Earth Plan.*
286 *Int.*, 154, 148-167.

287

288 Grosser, H., and other 11 co-authors, (1998). The Erzican (Turkey) earthquake (Ms 6.8)
289 of March 13, 1992 and its aftershocks sequence, *Pure Appl., Geophys.*, 152, 465-505.

290

291 Halldorsson, B., A. S. Papageorgiou (2005). Calibration of the specific barrier model to
292 earthquakes of different tectonic regions, *Bull. Seism. Soc. Am.*, 95, 4, 1276-1300.

293

294 Hanks, T., (1979). b values and $\omega^{-\gamma}$ seismic source models: implications for tectonic
295 stress variations along active crustal fault zones and the estimation of high-frequency
296 strong ground motion. *J. Geophys. Res.*, 84, 2235-2242.

297

298 Kanamori, H., (1977). The energy release of great earthquakes, *J. Geophys., Res.*, 82,
299 2981-2987.

300

301 Konno, K., and T. Ohmachi (1998). Ground-motion characteristic estimated from
302 spectral ratio between horizontal and vertical Components of Microtremor, *Bull. Seism.*
303 *Soc. Am.*, 88, 228-241.

304

305 Paige, C. C., and M. A. Saunders (1982). An algorithm for sparse linear equations and
306 sparse least squares, *ACM Trans. Math. Soft.*, **8**, 43-71.

307

308 Parolai, S., D. Bindi., M. Baumbach, H. Grosser., C. Milkereit, S. Karakisa, S. Zünbül
309 (2004). Comparison of different site response techniques using aftershocks of the 1999
310 Izmit earthquake, *Bull. Seism. Soc. Am.*, 94, 1096-1108.
311

312 Parsons, T. (2004). Recalculated probability of $M \geq 7$ earthquakes beneath the Sea of
313 Marmara, Turkey, *J. Geophys. Res.*, vol 109, B05304, doi:10.1029/2003JB002667.
314

315 Purvance, M. D., and J.G. Anderson (2003). A comprehensive study of the observed
316 spectral decay in strong-motion accelerations recorded in Guerrero, Mexico, *Bull. Seism.*
317 *Soc. Am.*, 93, 600-611.
318

319 Stromeyer, D., G. Grünthal., and R. Wahlström, (2004). Chi-square regression for
320 seismic strength parameter relations, and their uncertainties, with applications to an Mw
321 based earthquake catalogue for central, northern and northwestern Europe, *J. of*
322 *Seismology*, 8, 143-153.
323

324 Tibi, R., G. Bock, Y. Xia, M. Baumbach, H. Grosser, C. Milkereit, S. Karakisa, S.
325 Zünbül, R. Kind, and J. Zschau (2001). Rupture process of the 1999 August 17 Izmit and
326 November 12 Düzce (Turkey) earthquakes, *Geophys. J. Int.*, 144, F1-F7.
327

328 Wessel, P., and W.H.F. Smith (1991). Free software helps map and display data, *EOS.*
329 *Trans. AGU*, 72, 441, 445-446.

330 **Figure captions**

331

332 **Figure 1:** Top. Epicenter location (circles), seismological GTF and SABO (triangles) and
333 strong motion (KOERI) stations (squares). Bottom: Epicenter to seismic station ray paths
334 (black lines). Epicenter to strong-motion station ray paths (gray lines).

335

336 **Figure 2:** Top. Displacement spectra (black line) for M_L 5.5 and 2.1 earthquakes. The best fit
337 spectra obtained by the grid search procedure (step 1) are indicated by the gray lines.

338 Bottom. Acceleration spectra (black lines) for M_L 5.5 and 2.1 earthquakes. The best fit spectra
339 obtained by the grid search procedure (step 2) are indicated by the gray lines.

340

341 **Figure 3:** Top. κ values versus M_L . Bottom. *rms* versus M_L after step 1 (grey circles). *rms*
342 versus M_L after step 2 (black circles).

343

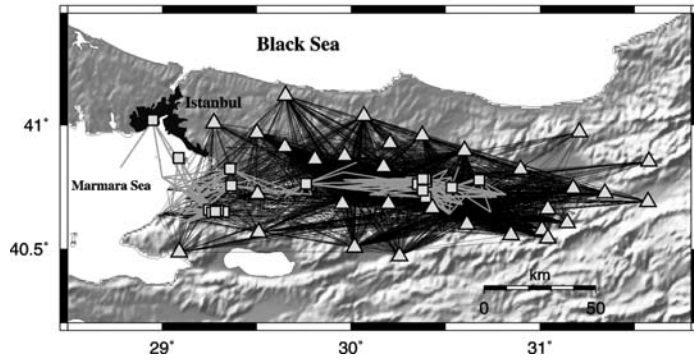
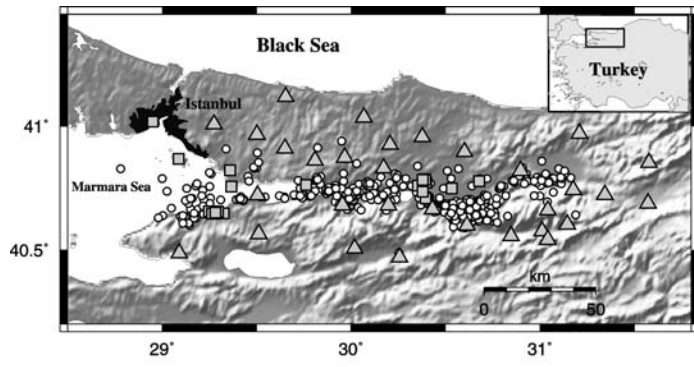
344 **Figure 4:** Top. f_c versus M_L . Bottom. $\log_{10}M_0$ versus source radius R . Line (black) of constant
345 $\Delta\sigma_B$ between 0.01 MPa (0.1 bar) and 10 MPa (100 bar) are shown.

346

347 **Figure 5:** $\Delta\sigma_{rms}$ versus $\Delta\sigma_B$.

348

349 **Figure 6:**Top. $\log_{10}M_0$ versus M_L (squares). Equation (3) from this study (black line), *Grosser*
350 *et al.*, (1998) (gray line), and *Durukal and Catalyürekli*, (2004) (dashed line). Bottom. M_w
351 versus M_L (squares) . Equation (4) from this study (black line), and *Stromeyer et al.* (2004)
352 (gray line).



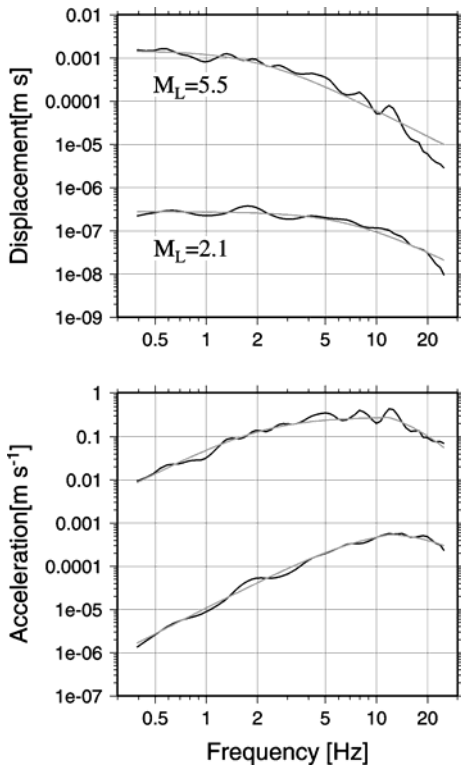
353

354

355

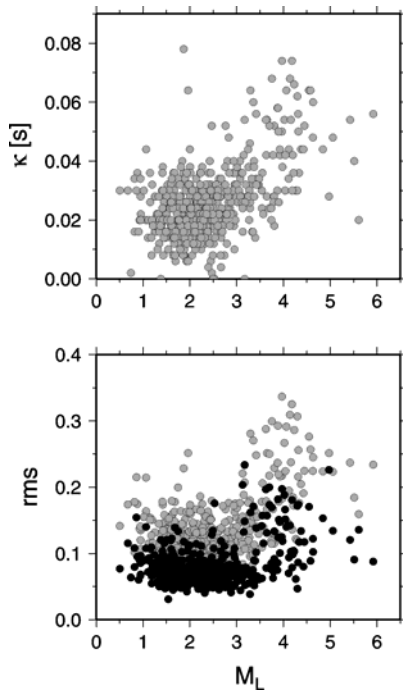
Figure 1:

356
357



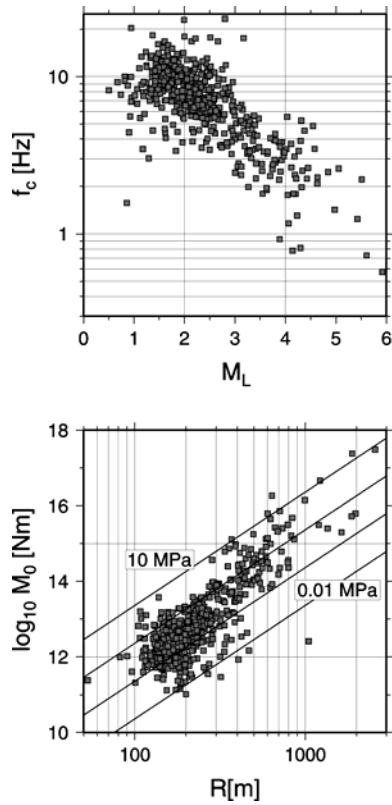
358
359
360
361
362
363
364
365
366

Figure 2.



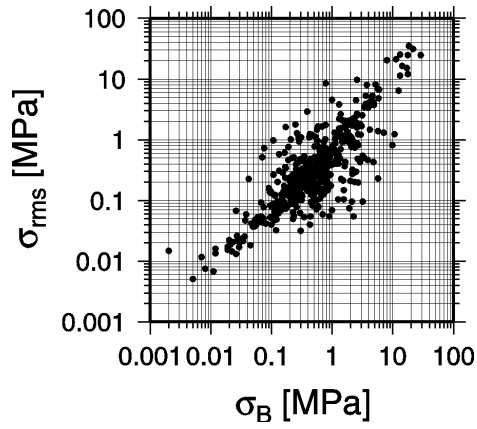
367
368
369

Figure 3.



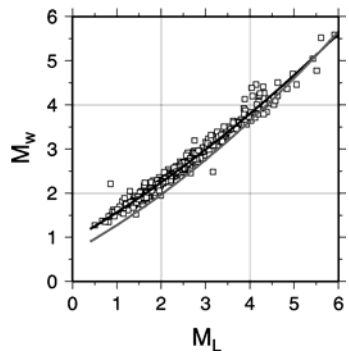
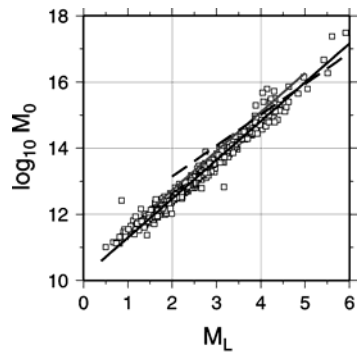
370
 371
 372
 373
 374
 375

Figure 4.



376
 377
 378
 379

Figure 5.



380
381
382
383

Figure 6.